ELSEVIER

Contents lists available at ScienceDirect

Dyes and Pigments

journal homepage: http://www.elsevier.com/locate/dyepig





Peptoid-phthalocyanine architectures with different grafting positions: Synthetic strategy and photoproperties

Maha Rzeigui ^{a, b}, Zeynel Şahin ^c, Olivier Roy ^a, Tuğba Küçük ^c, Ömer Göler ^c, Devrim Atilla ^c, Jameleddine Khiari ^{b, *}, Fabienne Dumoulin ^{c, d, **}, Claude Taillefumier ^{a, ***}

- ^a Université Clermont Auvergne, CNRS, SIGMA Clermont, ICCF, F-63000, Clermont-Ferrand, France
- b Université de Carthage, Faculté Des Sciences de Bizerte, Laboratoire de Chimie Organique et Analytique, ISEFC, 2000, Bardo, Tunisia
- Gebze Technical University, Chemistry Department, Gebze, 41400, Kocaeli, Turkey
- ^d Acıbadem Mehmet Ali Aydınlar University, Faculty of Engineering, Department of Medical Engineering, Istanbul, Turkey

ARTICLE INFO

Keywords:
Peptoid
Phthalocyanine
Helix
Conjugate

ABSTRACT

A monoazido Zn phthalocyanine has been grafted onto three different alkynyl-functionalized peptoid helices using copper-catalyzed azide–alkyne cycloaddition, demonstrating the feasibility of such conjugates. Their photoproperties have been examined relatively to the spatial geometry induced by the peptoid helix.

1. Introduction

Porphyrinoids are aromatic macrocycles with an extended electronic delocalization, conferring sought-after electronic and spectroscopic properties, amongst others [1]. Many biomolecules such as chlorophylls [2], hemes [3] and vitamin B12 [4] are natural porphyrinoid derivatives. The most common porphyrinoids are porphyrins and phthalocyanines, used in several applications fitting the preoccupations of our modern world, such as artificial photosynthesis [5], catalysis [6] and photocatalysis [7], photosensitisers for photodynamic therapy [8], conversion of light into electric current [9], amongst others. Many of these applications require multi-porphyrinoids arrays, often to promote photoinduced electron [10] or energy [11] transfers or also mimick the antennas in the photosynthetic reaction center of photosystems [12]. Several strategies have been developed to prepare multi-porphyrinoids arrays, either by using covalent (possibly conjugated) bonds [13,14], self-assemblies [15–17] or supramolecular edifices [18]. Peptoid backbones have been used recently to prepare cofacial arrays of two por-

Peptoids (*N*-substituted glycine oligomers) [20] are a special class of peptide mimics with desirable pharmacokinetic characteristics [21], including resistance against enzymatic degradation [22]. They can be

synthesized in a sequence-specific manner with hundreds of different side chains, thanks to the submonomer method [23] which uses primary amines as a source of side chains diversity [24]. For these reasons, they have been investigated for numerous biological applications [25]. The supramolecular assembly properties of peptoids also lead researchers to envisage their application as biomaterials [26]. The side chains of peptoids are appended to the amide nitrogen atoms rather than to the α-carbons, resulting in tertiary amide bonds. Unlike the peptide secondary amide bonds that are trans, with the exception of the prolyl-amide bonds, the peptoid tertiary amide bonds can adopt both the cis and trans conformations, one of the major cause of peptoid chain conformational flexibility [27]. Great efforts have been devoted to controlling the cis/trans isomerization of peptoid amides [28]. This allowed the identification of predictable discrete secondary structures, i. e. peptoid foldamers [29]. Some foldamers are based on a defined combination of backbone cis and trans amides [30], whereas others comprise only trans [31] or cis-amides [32]. It is now well established that peptoids with bulky α-chiral side chains adopt a helical conformation resembling the all-cis polyproline I (PPI) helix, with a 3-fold periodicity and a pitch of approximately 6 Å. The handedness of a peptoid PPI-type helix is governed by the side chains stereochemistries. (S)α-chiral side chains induce right-handed helices while the R

E-mail addresses: jamelkhiari@yahoo.fr (J. Khiari), Fabienne.Dumoulin@acibadem.edu.tr (F. Dumoulin), claude.taillefumier@uca.fr (C. Taillefumier).

^{*} Corresponding author. Gebze Technical University, Chemistry Department, Gebze, 41400, Kocaeli, Turkey.

^{**} Corresponding author. Gebze Technical University, Chemistry Department, Gebze, 41400, Kocaeli, Turkey

^{***} Corresponding author.

 $^{^{1}}$ (valid until 31 December 2019 for F.D.)

configuration induces the left-handed one. The most widely-used α -chiral side chains are aromatic, especially the phenylethyl (pe) [33] and 1-naphthylethyl (1npe) side chains [32a]. Beside their bulkiness, it has been reported that local $n \rightarrow \pi^*$ interactions between backbone carbonyls and the aromatic groups might be operative for stabilizing the cis-amides required for peptoid helix formation [28a-c]. The presence of one or several aromatic helical faces may also contribute to the conformational stability of peptoids [33a]. By contrast, very few studies have so far been undertaken to achieve conformationally stable peptoid PPI-type helices from non-aromatic monomers [32b,34]. Recently, we demonstrated that the very bulky tert-butyl (tBu) and α -gem-dimethyl groups do provide exclusively the cis-amide geometry [35]. Another side chain proposed by us with structure-inducing properties is the α -chiral 1-tert-butylethyl group (1tbe). An octamer sequence consisting of NtBu and Ns1tbe monomers in equal proportion provided a very stable PPI-type helix, the longest linear peptoid ever solved by X-ray crystallography [32b].

So far, the insertion of one or several porphyrins on peptoid scaffolds has been performed to optimize the cellular uptake efficiency of photosensitising porphyrins [36,37] or mimic the protein–chlorophyll ensemble found in photosynthetic antenna [38]. Jiwon Seo and his team beautifully used peptoid scaffolds to control porphyrin interactions, in the case of pure [19,39] or mixed [40–42] porphyrinic arrays.

In this work, the construction of conformationally stable PPI-type helices is sought after as topological templates to display phthalocyanine arrays. As such architectures are entirely new, this exploratory work aims at demonstrating the synthetic feasibility of such hybrids, at investigating the effect of the peptoid on the photoproperties of the phthalocyanine core, and at assessing the efficiency of the peptoid backbone in controlling the topology of dimeric phthalocyanine arrays.

2. Results and discussion

2.1. Molecular design

All the hybrid structures designed in the framework of these investigations are represented in Fig. 1. The first conjugate 1 made of a single phthalocyanine on a pentapeptoid scaffold was prepared to evaluate the effect of the presence of a peptoid scaffold on the photoproperties of the phthalocyanine core. Hybrids 2 and 3 have each 2 phthalocyanines grafted on a nonameric peptoid scaffold, with two residues between the two phthalocyanines in hybrid 2, and only residue between the two phthalocyanines in hybrid 3. Phthalocyanine 4 will be used as the pristine reference phthalocyanine macrocycle.

The phthalocyanine core was chosen taking into account several considerations: Zn phthalocyanines have interesting photophysical and photochemical properties which can be tailored by their substitution pattern [43], and O-hexyl non-peripheral substitution is known to ensure of a satisfying solubility in common organic solvents [44].

The sequence design of the oligomers lies on the 3-fold periodicity of the PPI-like helix. The aliphatic *Ns*1tbe monomers have been chosen as helical structure inducers (Fig. 2). Rather than aromatic side chains likely to interact with the phthalocyanine moieties, aliphatic side chains have been chosen, also because among all the aliphatic side chains tested so far the chiral bulky s1tbe side chain have achieved the best performance as helical structure inducer. Three peptoid oligomers have been selected: one pentamer (5) and two nonamers (6 and 7), each with an acetamide and a carboxamide group at the *N*- and *C*-termini (Table 1). The pentamer 5 comprises a (propargyl side chain as the central residue, flanked on each side by two *Ns*1tbe residues. Both nonamers are composed of seven *Ns*1tbe and two *Nem* (*N*-ethynylmethyl glycine) residues. In the sequence of 6, the propargyl side chains are

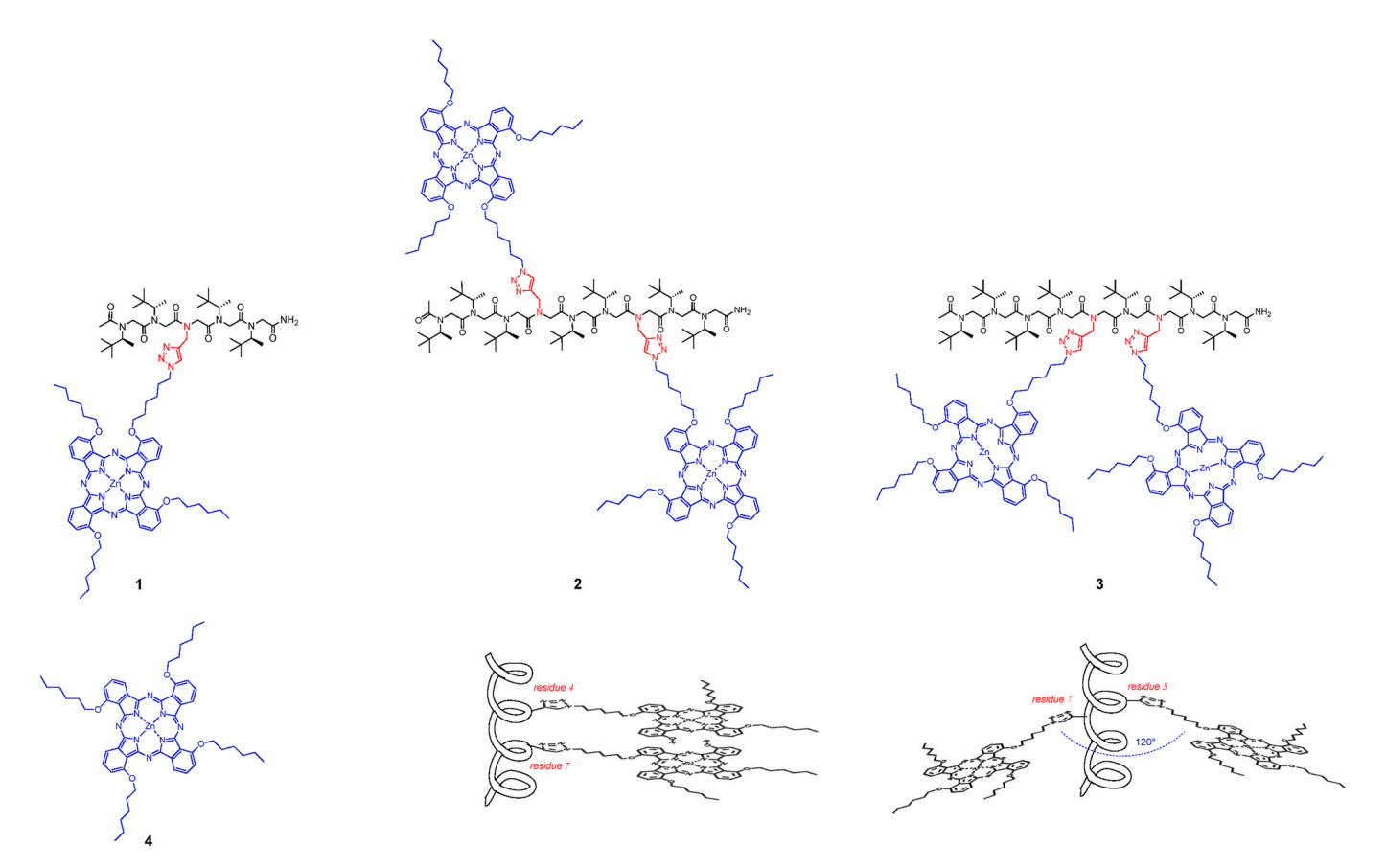


Fig. 1. Structures of the peptoid-phthalocyanine architectures 1–3 (with their expected topology) and of reference phthalocyanine 4. For each phthalocyanine, only one of the existing isomers is shown.

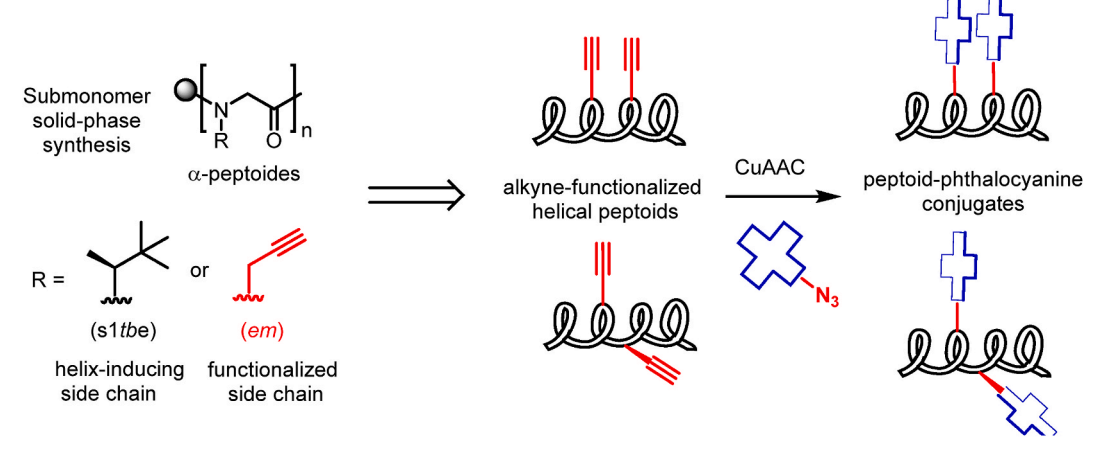


Fig. 2. Retrosynthetic strategy for the preparation of the targeted peptoid-phthalocyanine conjugates.

Table 1Sequence, purity, and mass spectra data of the peptoids 5–7.

peptoid	monomer sequence ^a	overall yield ^b	% purity ^c	expected mass	observed mass
5	NH2	57	96	718.54	719.54 [M+H] ⁺
6	Ac-Ns1tbe-Ns1tbe-Ns1tbe-Ns1tbe-NH ₂	46	94	1236.92	1237.92 [M+H] ⁺
	Ac-(Ns1tbe) ₃ -Nem-(Ns1tbe) ₂ -Nem-(Ns1tbe) ₂ -				
7	NH ₂	56	94	1236.92	1237.92 [M+H] ⁺
	Ac-(Ns1tbe) ₄ -Nem-Ns1tbe-Nem-(Ns1tbe) ₂ -				
	NH_2				

^a The peptoids were drawn with amides in the *trans* conformation by ease of drawing.

appended on residues 4 and 7 (i and i+3), thus the two functional side chains are expected to be on the same face of the helix. For the nonamer 7, the two Nem residues correspond to the residues 5 and 7 of the sequence. Consequently, based on the three-fold periodicity, the propargyl side chains are expected to form a 120° degree angle.

The synthetic strategy was conceived as detailed on Fig. 2. To anchor the phthalocyanines onto the peptoid scaffold, the copper(I)-catalyzed alkyne-azide cycloaddition (CuAAC) was chosen for its great versatility [45–47] and the easy access to azide-functionalized phthalocyanines. This implied the introduction of peptoid side chains containing an alkyne function, which we have demonstrated to be achievable [48]. Another expected advantage is that the formed 1,2,3-triazole linker is also, at least to some extent, a *cis*-amide inducer [28c], which may help folding the peptoid chain of the conjugate compounds.

2.2. Synthesis and characterization

2.2.1. Propargyl-functionalized peptoid scaffold

Peptoids are commonly synthesized on solid support by the submonomer method pioneered by Zuckermann [23]. In this method, each new monomer is constructed in two iterative steps: (1) bromoacetylation of the *N*-terminus of the growing chain, (2) introduction of the side chain by bromine atom displacement of the formed bromoacetamide by a primary amine. This process is most often very efficient, yielding to pure peptoids in high yields. The major limitation may originate from the steric hindrance of the formed *N*-terminus secondary amine which may impair chain elongation efficiency. In this work, the solid-phase synthesis of peptoid oligomers comprising *Ns*1tbe monomers was evaluated for the first time. The optimized conditions for the synthesis of

 $^{^{\}rm b}$ Based on the resin loading (0.52 mmol g $^{\rm -1}$), include all the solid-phase steps and the final acetylation in solution.

 $^{^{\}rm c}\,$ Determined by integration of the high-performance liquid chromatography (HPLC) UV trace at 214 nm.

peptoids 5-7 are depicted in Scheme 1.

The syntheses were performed manually using a Fmoc-protected Rink amide MBHA resin as the support, leading to C-terminus carbox-amides upon cleavage. After several round of optimizations, we found that conducting the two steps of the submonomer protocol under gentle warming (40 °C) had a beneficial effect on the purity of the peptoids. Other important improvements concern the acylation step and the substitution reactions with the bulky (2S)-3,3-dimethylbutan-2-amine (s1tbe amine) which were systematically repeated with new amount of reagents. The final acetylation of the peptoids was carried out in solution (Ac₂O, Et₃N), after cleavage from the resin, and the compounds were purified by flash chromatography on silica gel. We have indeed observed that the cleavage of the acetylated resin-bound peptoids under acidic conditions led to the loss of one residue at the N-extremity of the oligomers (Table 1).

2.2.2. Conformational studies

The helical character of the three peptoids 5-7 was assessed by Circular Dichroism (CD) in methanol (Fig. 3). The three peptoids display the typical signature associated with the PPI-type helical conformation of peptoid oligomers bearing aliphatic side chains. It is worth noting that peptoids with α -chiral aromatic side chains exhibit a completely different profile resembling that of the peptide α -helix. In our case, the Sconfiguration of the s1tbe side chains produces CD curves with the same right-handed helicity as those of poly-(L-prolines) in alcohol solvents. The curves are characterized by a positive maximum at around 210 nm and two minima at 190 and 225 nm. The strong intensities of ellipticity on a per-residue molar basis, at 210 nm for the two nonamers, as compared to literature data, are indicative of well-structured compounds and likely also reflect a cooperative folding process. Unsurprisingly, the short length pentamer is less structurally stable; protohelical structures are generally observed from the tetramer length. Measurements at the Q band wavelength were not expected to be meaningful due to the high concentrations used to record CD and the subsequent aggregation affecting their absorption at this wavelength, unlike porphyrins that are much less prone to aggregation¹⁹.

As the degree of PPI helical conformational order depends on the population of cis-amide bonds, we also estimated overall backbone amide $K_{cis/trans}$ values. As recently described by us, the calculations were made on the basis of the NMR integration (2D-HSQCAD experiments, Fig. 4) of the methyne protons of the s1tbe side chains, which show distinct resonances depending on the cis or trans conformation of the amides (Supporting information). This calculation does not take into account the amide bonds connecting the Nem residues with their

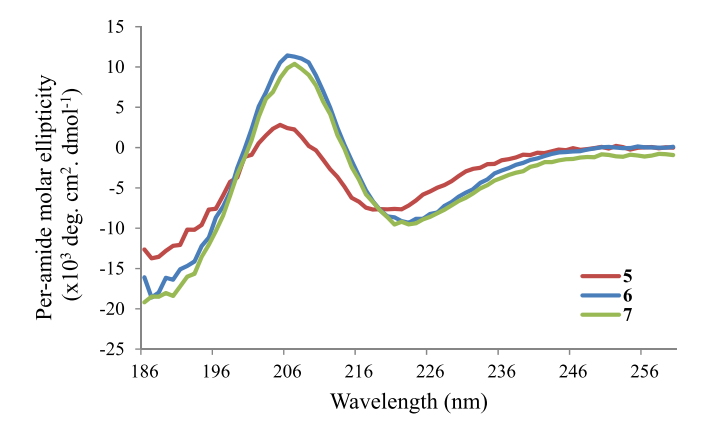


Fig. 3. CD spectra of peptoid oligomers 5-7 in MeOH at 500 μM .

preceding residues, which corresponds to one in five amide bonds in the case of the pentamer **5**, and two in nine amides in the case of the nonamers **6** and **7**. The overall proportion of *cis*-amide determined for the amide bonds connecting the *Ns*1tbe residues with their preceding residue was found to be 93% for the pentamer **5** ($K_{cis/trans} = 13.2$), and 95% for the nonamer **6** ($K_{cis/trans} = 21.5$). The *trans*-amide rotamers were no longer detectable in the case of nonamer **7**, it can be confidently considered that the proportion of *cis*-amides >98% ($K_{cis/trans} > 49.0$) in this case. These results confirm the high helical character of the nonamer peptoids, the lower degree of structuration of the pentamer, as seen from CD, appears to be correlated to a substantial conformational heterogeneity arising from *cis/trans* amide bond isomerization.

2.2.3. Synthesis of azidophthalocyanine

Azidophthalocyanines, especially when an asymmetric substitution pattern, are often prepared from corresponding hydroxylated phthalocyanines, via successive mesylation then azidation. Hence monohydroxylated phthalocyanine 10 was first prepared from phthalonitriles 8 and 9, reference phthalocyanine 4 being produced concomitantly. The significant difference in polarity of both phthalocyanines allowed the quite easy separation by silica gel chromatography. Monohydroxylated phthalocyanine 10 was first mesylated, and the crude product was immediately reengaged without further purification in the nucleophilic substitution by sodium azide, yielding phthalocyanine 11 (Scheme 2).

2.2.4. Peptoid-phthalocyanine conjugates 1-3

Access to the three conjugates 1-3 by copper-catalyzed azide-alkyne

Scheme 1. Solid-phase submonomer synthesis of peptoids 5–7 (optimized conditions). Acylation step: BrCH₂CO₂H (6 equiv., 0.4 M/DMF), diisopropylcarbodiimide (DIC, 8 equiv., 2 M/DMF), 2×5 min at 40 °C. Substitution step: 25 equiv. of HC \equiv CCH₂NH₂, 2 M/DMF, 1 h at 40 °C or 15 equiv. of tBuCH(CH₃)NH₂), 2 M/DMF, 2 × 1 h at 40 °C. Cleavage: TFA/DCM (95/5), RT, 10 min. Acetylation: Ac₂O (4 equiv.), Et₃N (2 equiv.), EtOAc (0.2 M), 18 h, RT.

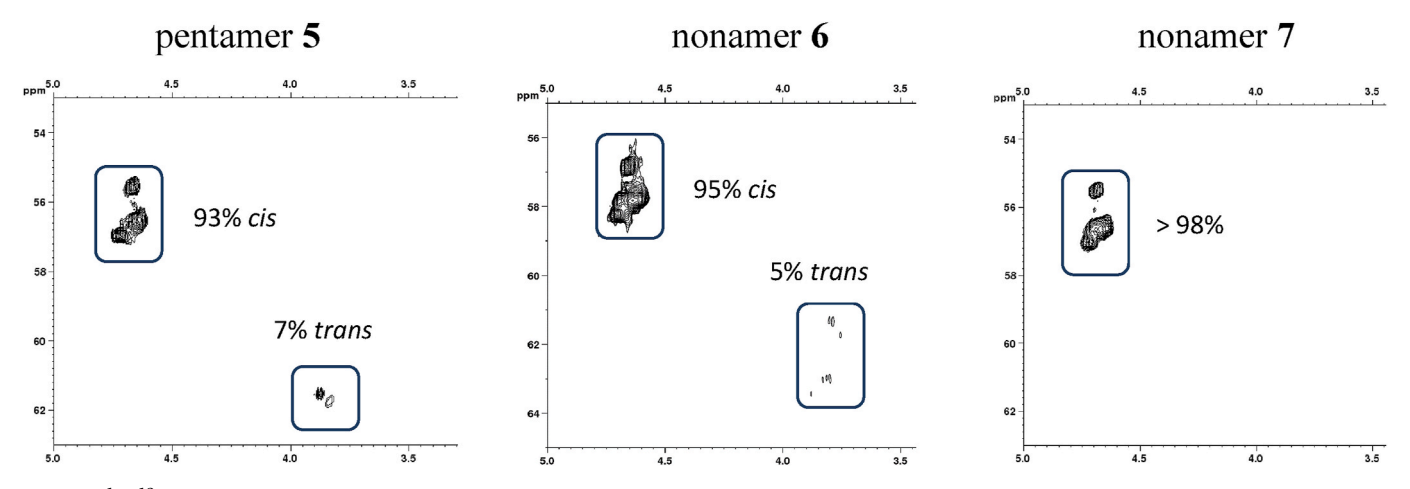
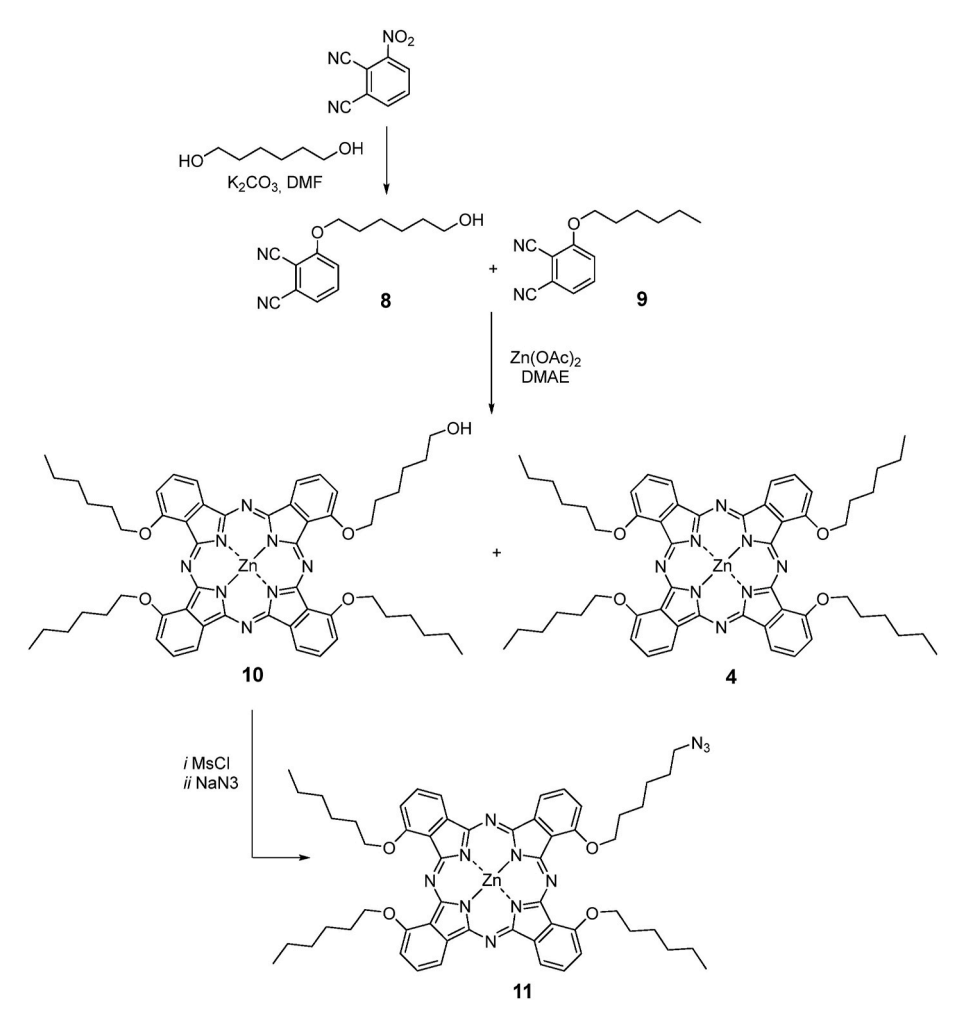


Fig. 4. 1 H- 13 C HSQCAD NMR spectra of peptoids 5–7. Panels display side chains Ns1tbe methyne protons. Peptoid concentration was \sim 10 mM in CD₃OD.



Scheme 2. Synthesis of azidophthalocyanine 11 and of the reference phthalocyanine 4. For each phthalocyanine, only one of the existing isomers is shown.

cycloadditions (CuAAC) was successfully achieved using ligand-free conditions. The azidophthalocyanine 11 and alkyne-functionalized peptoids were simply combined in presence of $CuSO_4$ and ascorbic acid in a biphasic CH_2Cl_2/H_2O solvent system known to increase CuAAC reaction rates (Scheme 3) [49]. The azidophthalocyanine 11 was used in a 1.5-fold excess per alkyne functional group to facilitate peptoid conversion. The three conjugates were first purified on silica gel to remove excess azidophthalocyanine 11, and then by size-exclusion

chromatography, using THF or dichloromethane as eluent, to eliminate residual amount of starting peptoids.

CD analysis of peptoid backbone is based on the amide chromophore in the far UV region (240-180 nm), which necessitates the use of UV-transparent solvents, typically, acetonitrile, methanol and water. Unfortunately, the poor solubility of peptoid-phthalocyanine conjugates 1–3 in these solvents prevented their CD analysis.

Interestingly, we were able to determine the peptoid amide $K_{cis/trans}$

Scheme 3. Synthesis of the peptoid-phthalocyanine conjugates 1–3. For each phthalocyanine, only one of the existing isomers is shown.

for the three conjugates, from $^{1}H^{-13}C$ -HSQCAD experiments in deuterated dichloromethane (Fig. 5). As previously, the methyne cis and trans peaks of the s1tbe side chains were integrated for $K_{cis/trans}$ determination. We observed a dramatic decrease (84%) in average $^{Ns1tbe}K_{cis/trans}$ value for the shorter peptoid oligomer conjugate 1 $(cis/trans \text{ ratio } \sim 2:1)$, relative to its parent peptoid 5 (>13:1). By contrast, peptoid amide isomerism was not significantly affected in the conjugates 2 and 3 relative to peptoid nonamers 6 and 7, respectively. Interestingly, the

conformational homogeneity is even increased for the conjugate **2**, for which the *trans* rotamers are no longer detectable. The opposite is observed for the conjugate **3** relative to **7**. A small proportion of *trans*-amide rotamers (4%) are observed for **3**, while the parent nonamer **7** was completely homogeneous in term of amide rotamerism. Overall, the conformational homogeneity of the two peptoid-phthalocyanine conjugates **2** and **3** is remarkable, especially considering the size of the phthalocyanine moieties relative to the peptoid templates, and also, the potential intra- and inter-molecular interactions they can establish. The unique conformation known for peptoids displaying all-*cis* amides is the PPI helix, the most likely outcome for the two nonameric conjugates.

2.3. UV-vis spectroscopy

The photoproperties of phthalocyanines are depending on structural factors (metal, nature, number and position of substituents) as well as on external parameters such as the solvent, concentration and temperature. As all compounds 1–4 have the same phthalocyanine core, and for the sake of comparisons, UV–vis spectra of 1–4 have been first recorded in different solvents. As derivatives 2 and 3 have twice the amount of phthalocyanines, 2 μM concentrations were used for 2 and 3 whereas 4 μM concentrations were used for 1 and 4 (Fig. 6). The maximum absorption for the Q band in each solvent is summarized in Table 2, together with the extinction coefficient values. Spectra used to determine these values are displayed in the supplementary material (Figs S1-16).

The first observation is that the presence of a peptoid helix and of the triazole ring does not affect by itself the photoproperties of the phthalocyanine macrocycle, as can be deduced when comparing spectra of 1 and 4, whose spectra have roughly the same shape and intensity in all solvents, with the presence of H-aggregates in chlorinated solvents characterized by the apparition of a red-shifted second Q band in THF and DMF. Conjugates ${\bf 2}$ and ${\bf 3}$ are very aggregated in dichloromethane and in chloroform, as evidenced by their large and potato-shaped Q band. In THF and DMF, their Q band is sharper but the absorption is much less intense than for 1 and 4. As the overall concentration of phthalocyanines is the same in all the samples, one can infer that it is due to their spatial proximity induced by the grafting of two phthalocyanine units on a same peptoid backbone, who therefore interact with each other. The position of the phthalocyanine on the peptoid backbone does not affect significantly this phenomenon. Even though the helix retains its conformation after the grafting, the flexibility of the C6 spacer between the peptoid backbone and the phthalocyanine core provide enough freedom of movement to the two macrocycles whose π - π stacking occurs similarly for both conjugates 2 and 3 in dichloromethane and chloroforme. Tetrahydrofuran and N,N-dimethylformamide both appear

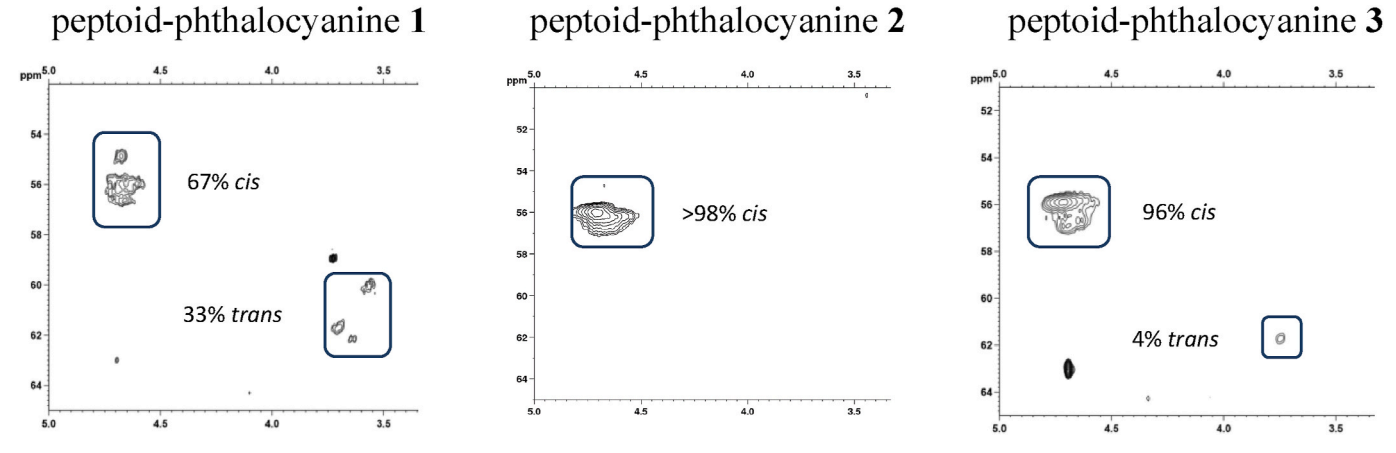


Fig. 5. $^{1}H^{-13}C$ HSQCAD NMR spectra of peptoids 1–3. Panels display side chains Ns1tbe methyne protons. Peptoid concentration was \sim 5 mM in deuterated dichloromethane.

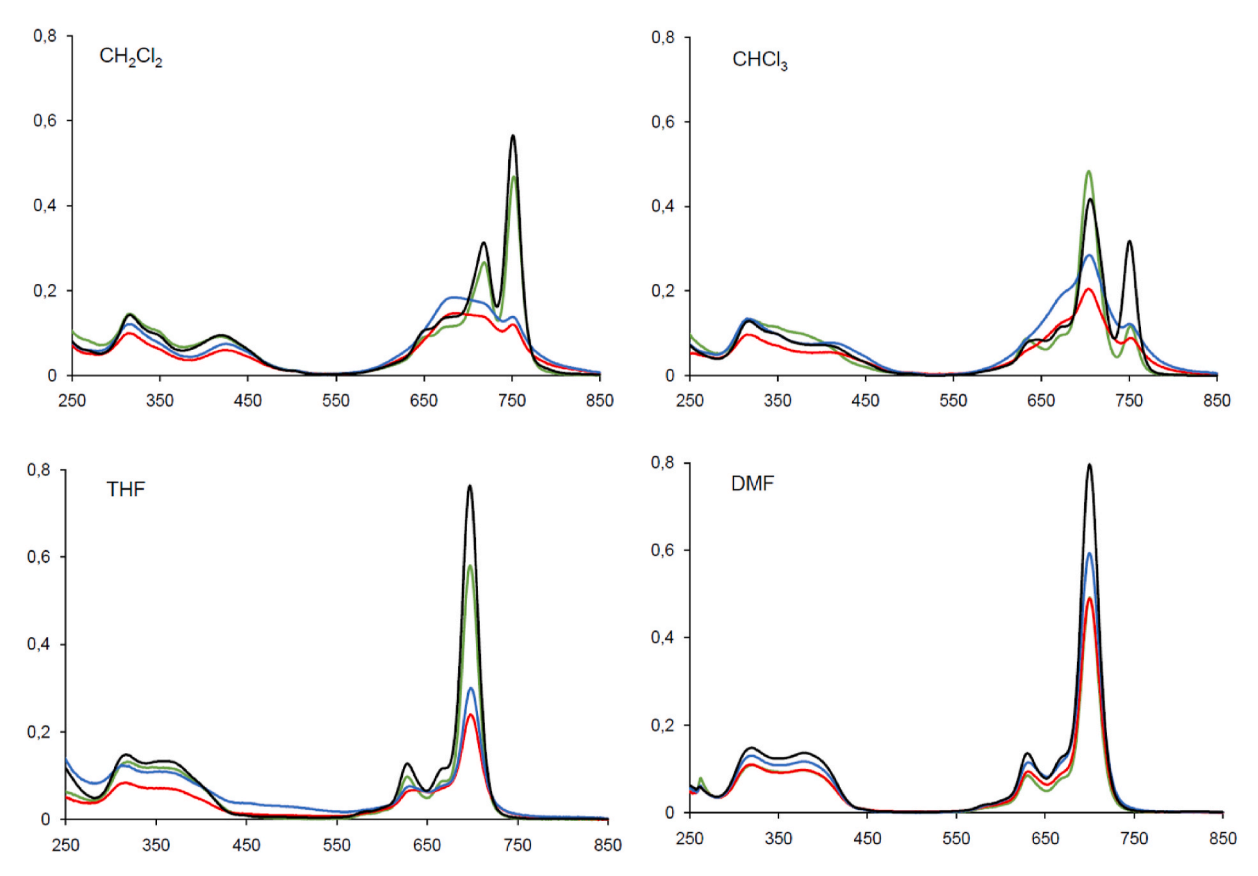


Fig. 6. Superimposed UV–vis spectra of 1 (green, 4 μ M), 2 (red, 2 μ M), 3 (blue, 2 μ M) and 4 (black, 4 μ M) in dichloromethane (top left), chloroforme (top right), tetrahydrofurane (bottom left) and dimethylformamide (bottom right). (For interpretation of the references to colour in this figure legend, the reader is referred to the Web version of this article.)

Table 2 UV-visible data

Compound	Solvent	λ_{max} Q band (nm)	log E
1	CH ₂ Cl ₂	752	5.1
	CHCl ₃	704	5.1
	THF	698	5.2
	DMF	700	5.1
2	CH ₂ Cl ₂	683	4.9
	CHCl ₃	704	5.0
	THF	698	5.0
	DMF	700	5.4
3	CH ₂ Cl ₂	682	5.0
	CHCl ₃	704	5.1
	THF	698	5.2
	DMF	698	5.5
4	CH ₂ Cl ₂	751	5.2
	CHCl ₃	705	5.1
	THF	697	5.3
	DMF	700	5.3

to inhibit this intramolecular aggregation, in line with previous general observations on phthalocyanines.

2.4. Fluorescence

Fluorescence has been recorded in THF to explore more in detail the behaviour of the set of compounds, as it known to be a more sensitive technique. Spectra are displayed on Fig. 7 and data are gathered in Table 3.

At the working concentrations (normalized at absorption 0.2), a

significant effect of the sole presence of the peptoid helix is observed when comparing 1 and 2. The fluorescence quantum yield (Φ_F) of 1 is indeed only 2/3 of those of the reference phthalocyanine 4. When comparing the data for 3 and 4, Φ_F value is significantly lower than for the monomeric derivatives, and is interestingly slightly higher for 2 than for 3, even though the helix of conjugate 2 is more likely to promote intramolecular interactions as it would promote co-facial geometry. It confirms the fact the phthalocyanines have enough freedom of movement and hence that their relative configuration is not much affected by the helix configuration but rather by being maintained close to each other by the grafting on the same peptoid backbone.

3. Experimental

3.1. Materials and methods

Synthesis and analysis of compounds 1–3 and 5–7: THF, CH_2Cl_2 were dried over aluminum oxide via a solvent purification system. EtOAc, CH_2Cl_2 , cyclohexane, and MeOH for column chromatography were obtained from commercial sources and were used as received. All other solvents and chemicals obtained from commercial sources were used as received. NMR spectra were recorded on a 400 MHz Bruker Avance III HD spectrometer. Chemical shifts are referenced to the residual solvent peak and J values are given in Hertz. The following multiplicity abbreviations are used: (s) singlet, (bs) broad singlet, (d) doublet, (t) triplet, (q) quartet, (m) massif, and (br) broad. TLC was performed on Merck TLC aluminum sheets, silica gel 60, F254. Visualizing of spots was effected with UV-light and vanillin in EtOH/H₂SO₄, or ninhidrin or phosphomolybdic acid in EtOH. Flash chromatography was performed with Merck silica gel 60, 40–63 μ m. HRMS was recorded on a Micromass Q-Tof Micro (3000 V) apparatus or a Q Exactive Quadrupole-Orbitrap

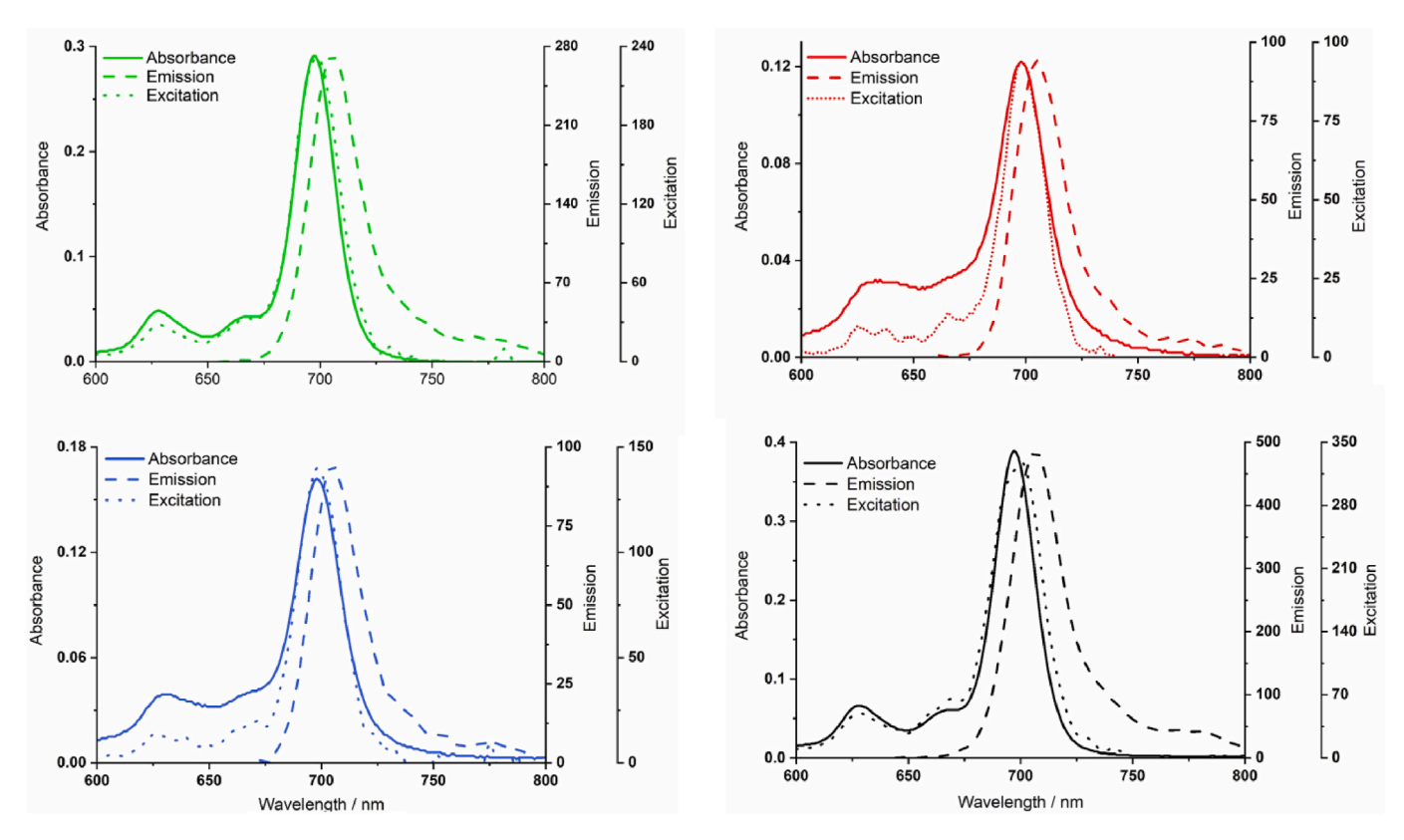


Fig. 7. Normalized fluorescence spectra of compounds 1 (green), 2 (red), 3 (blue) and 4 (black) in tetrahydrofuran. (For interpretation of the references to colour in this figure legend, the reader is referred to the Web version of this article.)

Table 3 Fluorescence data

	Excitation λ_{Ex} (nm)	Emission λ_{Em} (nm)	Stokes shift Δ_{Stokes} (nm)	Φ_{F}
1	698	705	7	0.168
2	698	705	7	0.098
3	698	705	7	0.074
4	700	707	10	0.270

Mass Spectrometer. LC–MS was recorded a Q Exactive Quadrupole-Orbitrap mass spectrometer coupled to a UPLC Ultimate 3000 (Kinetex EVO C18; $1.7~\mu m; 100~mm \times 2.1~mm$ column with a flow rate of 0.45 mL min–1 with the following gradient: a linear gradient of solvent B from 5% to 95% over 7.5 min (solvent $A=H_2O+0.1\%$ formic acid, solvent B= acetonitrile + 0.1% formic acid) equipped with a DAD UV/ vis 3000 RS detector.

Synthesis of compounds 4 and 8-11: All solvents and reagents were of reagent grade quality and obtained commercially from Aldrich, Fluka or Merck. Phthalonitrile 9 [44] and 3-nitrophthalonitrile [50] were prepared as previously reported. Previously reported procedure for phthalonitrile 8 was slightly modified [51]. IR spectra were recorded between 4000 and 650 cm⁻¹ using a PerkinElmer Spectrum 100 FT-IR spectrometer. Mass spectra were recorded on a MALDI (matrix assisted laser desorption ionization) BRUKER Microflex LT using dithranol (DIT) or 2, 5-dihydroxybenzoic acid (DHB) as the matrix. High resolution mass spectra were measured on an Agilent 6530 Accurate-Mass Q-TOF LC/MS spectrometer equipped with electrospray ionization (ESI) source. NMR spectra of 4, 8, 10 and 11 were recorded in deuterated solvents (CDCl₃) on a Varian 500 MHz spectrometer at 298 K. Electronic absorption spectra were measured with a Shimadzu UV-2600 UV-vis spectrophotometer, and a Varian Cary Eclipse spectrofluorometer is used to record steady-state fluorescence emission spectra were recorded by using at room temperature, using 10 mm path length cuvettes. Details about the determination of the fluorescence quantum yields are provided in the supplementary material.

3.2. Synthesis of peptoid oligomers

Peptoid oligomers 5-7 were prepared by solid-phase submonomer synthesis. All steps were carried out manually in 5 mL plastic fritted syringes fitted with a stopcock. The syringes were placed on a benchtop orbital shaker for reaction incubations. Peptoids were synthesized on polystyrene resin with an Fmoc-protected Rink amide MBHA linker (Novabiochem 100–200 mesh; 0.52 mmol g^{-1}). The Fmoc-protected resin (0.150 g, 0.078 mmol) was swollen in DMF (2 mL) for 10 min. The swelling was repeated (2x). The Fmoc group was removed by soaking the resin in a 20% piperidine/DMF solution for 15 min at rt after which time the resin was washed with DMF (5 \times 2 mL) and drained. The deprotection reaction was repeated (1x). A solution of bromoacetic acid (65 mg, 0.46 mmol, 6 equiv) in DMF (1.2 mL) was added to the deprotected resin, followed by a solution of diisopropylcarbodiimide (DIC) (0.1 mL, 0.63 mmol, 8 equiv) in DMF (0.3 mL). The reaction was heated at 40 °C under stirring for 10 min. This acylation step was repeated (1x) when the growing chain was ended by a bulky N-tert butylethyl group. The resin was filtered, washed with DMF (5 \times 2 mL) and drained. A solution of amine (for s1tbe 0.16 mL/0.6 mL DMF 1.17 mmol, 15 equiv; for em 0.124 mL/0.6 mL DMF, 1.95 mmol, 25 equiv) added to the resin, and the reaction mixture was agitated at 40 °C for 1 h. This step was repeated (1x) in the case of a substitution by the (2S)-3,3dimethylbutan-2amine. The resin was filtered, washed with DMF (5 $\times\,2$ mL) and drained. This 2-steps sequence of acylation and substitution was repeated until the target oligomer was obtained. After the elongation steps, the resin was washed with CH_2Cl_2 (5 \times 2 mL) and drained. The peptoid was cleaved from the resin by stirring in 95% trifluoroacetic acid/CH2Cl2 (2 mL) for 10 min at rt. This cleavage procedure was repeated (1x). The resin was washed with CH_2Cl_2 (2 × 2 mL) and the

M. Rzeigui et al. Dyes and Pigments 189 (2021) 109095

filtrate evaporated under reduced pressure. The residual TFA was eliminated by adding ${\rm CH_2Cl_2}$ (5 mL) and evaporation. Identity of the peptoids was controlled by LC-MS (UV detection at 220 nm). The crude oligomers were acetylated in solution. The peptoid was dissolved in EtOAc (0.2 M) and cooled to 0 °C under Ar. Et₃N (2.0 equiv) was added to the stirring solution of amine, followed by addition of acetic anhydride (4 equiv) under Ar. After 2 h at 0 °C, the mixture was allowed to stand overnight at room temperature. The mixture was filtered, and the solids washed with EtOAc. The filtrate was then concentrated in vacuo, yielding the crude *N*-acetylated compound which was purified by flash column chromatography on silica gel. Purity was determined by HPLC (UV detection at 220 nm), and the product identity was confirmed by HRMS before CD and NMR analyses.

*Peptoid 5 (Ac-Ns1tbe-Ns1tbe-Nem-Ns1tbe-Ns1tbe-NH*₂). Pentamer 5 was isolated as a white solid after purification by flash column chromatography on silica gel. 32.8 mg (0.045 mmol) were obtained. R_f = 0.63 (9:1 CH₂Cl₂/MeOH). ¹H NMR (400 MHz, CDCl₃) δ (ppm): 0.76–1.41 (m, 48 H, CH(CH₃)C(CH₃)₃), 1.92–2.26 (m, 4 H, COCH₃ and C≡CH), 3.33–5.10 (m, 16 H, 5 × NCH₂CO, NCH₂C≡C and 4 × CH(CH₃) C(CH₃)₃), 5.52–7.95 (m, 2 H, CONH₂). HRMS (TOF MS ES+) m/z calcd for C₃₀H₇₁N₆O₆ [M+H] ⁺ 719.5429; found 719.5417.

Peptoid 6 Peptoid 6 was isolated as a white solid after purification by flash column chromatography on silica gel. 25.17 mg (0.020 mmol) were obtained. $R_f = 0.65$ (9:1 CH₂Cl₂/MeOH). ¹H NMR (400 MHz, CDCl₃) δ (ppm): ¹H NMR (400 MHz, CDCl₃) δ (ppm): 0.71–1.36 (m, 84 H, CH(CH₃)C(CH₃)₃), 1.92–2.17 (m, 3 H, COCH₃), 2.26–2.49 (m, 2 H, C≡CH), 3.47–4.88 (m, 29 H, 9 × NCH₂CO, 2 × NCH₂C≡C and 7 × CH (CH₃)C(CH₃)₃), 5.97–7.92 (m, 2 H, CONH₂). HRMS (TOF MS ES+) m/z calcd for $C_{68}H_{121}N_{10}O_{10}^{+}$ [M+H] ⁺ 1237.9262; found 1237.9267.

Peptoid 7 Peptoid 7 was isolated as a white solid after purification by flash column chromatography on silica gel. 54.2 mg (0.043 mmol) were obtained. R_f = 0.65 (9:1 CH₂Cl₂/MeOH). 1 H NMR (400 MHz, CDCl₃) δ (ppm): 0.62–1.37 (m, 84 H, CH(CH₃)C(CH₃)₃), 2.00–2.07 (m, 3 H, COCH₃), 2.26–2.39 (m, 2 H, C≡CH), 3.39–4.88 (m, 29 H, 9 × NCH₂CO, 2 × NCH₂C≡C and 7 × CH(CH₃)C(CH₃)₃), 5.97–7.92 (m, 2 H, CONH₂). HRMS (TOF MS ES+) m/z calcd for C₆₈H₁₂₁N₁₀O₁₀⁺ [M+H]⁺ 1237.9262; found 1237.9247.

3.3. Synthesis of azidophthalocyanine 11

Phthalonitrile 8. 3-Nitrophthalonitrile (3.46 g, 20 mmol), 1,6 hexanediol (100 mmol, 12.0 g) and $\rm K_2CO_3$ (500 mmol, 69 g) were stirred overnight at 60 °C in DMF (150 mL), then the reaction mixture was poured into water. The resulting white precipitate was filtrated and purified by column chromatography (silica gel) using CH₂Cl₂/EtOH (50/1) as the eluent. Yield: 53% (2.6 g). $\rm C_{14}H_{16}N_2O_2$, MW: 244.29 g/mol. FT-IR (ν , cm⁻¹): 3315, 3088, 2935, 2861, 2238, 2226, 1978, 1580, 1473, 1453, 1399, 1291, 1177, 1033, 923, 844, 795, 729, 684. ¹H NMR (500 MHz, CDCl₃) δ (ppm): 1.47 (2 H), 1.56 (m, 3 H), 1.90 (2 H), 3.67 (t, 2 H), 4.14 (t, 2 H), 7.21 (d, 1 H), 7.33 (d, 1 H), 7.62 (t, 1 H). ¹³C NMR (125 MHz, CDCl₃), δ (ppm): 25.58, 25.84, 28.81, 32.68, 62.91, 70.03, 110.01, 116.69, 117.37, 125.02, 134.57, 161.63.

Hydroxyphthalocyanine 10 and phthalocyanine 4. Phthalonitrile **8** (300 mg, 1.23 mmol), phthalonitrile **9** (1.4 g, 6.15 mmol), and zinc acetate (0.13 g, 0.61 mmol) were stirred at 140 °C for 18 h under argon atmosphere in dry dimethylaminoethanol (6 mL). After evaporation of the solvent, the residue was dissolved in dichloromethane and purified by column chromatography (silica gel) using $CH_2Cl_2/EtOH$ (20/1) as the eluent. Symmetrically substituted phthalocyanine **4** was first eluted, followed by the monohydroxylated AB_3 derivative **10**.

Symmetric phthalocyanine 4. Dark-blue waxy solid. 50 mg $C_{56}H_{64}N_8O_4Zn$, MW 978.56. ATR-IR: v_{max} (cm⁻¹) 2924, 2853 (aliph. C–H), 1594 (C=N). ¹H NMR (500 MHz, CDCl₃) δ ppm: 0.89–1.06 (m, 12 H, CH₃), 1.25–2.58 (m, 32 H, CH₂), 3.95–4.89 (m, 8 H, CH₂), 6.71–9.04 (m, 12 H, ArCH). ¹³C NMR (125 MHz, CDCl₃) δ ppm: 14.36, 22.98–32.44, 68.73–69.56, 68.55, 70.59, 110.31–157.47. Anal. calc. for

 $C_{56}H_{64}N_8O_4Zn:$ 68.74C, 6.59; H, 11.45; N %, Found: C, 68.50; H, 6.40; N, 11.20. MALDI-TOF: m/z 979.12 [MH] $^+$. HR-ESI-MS m/z: Calcd for $C_{56}H_{65}N_8O_5Zn:$ 977.4420, Found 977.4331.

Monohydroxyphthalocyanine 10. Dark-blue waxy solid. 20 mg C₅₆H₆₄N₈O₅Zn, MW 994.56. ATR-IR: $v_{\rm max}$ (cm⁻¹) 3410 (OH), 2924, 2853 (aliph. C–H), 1594 (C=N). 1 H NMR (500 MHz, DMSO- d_6) δ ppm: 0.81–1.01 (m, 9 H, CH₃), 1.26–1.78 (m, 24 H, CH₂), 1.85–2.31 (m, 10 H, CH₂), 3.50–3.58 (m, 1 H, OH), 4.07–4.94 (m, 8H, CH₂O), 7.27–8.25 (m, 12 H, ArCH). 13 C NMR (125 MHz, DMSO- d_6) δ ppm: 14.65, 22.73–33.40, 61.12, 61.44, 68.55, 70.59, 113.16–156.50. Anal. calc. for C₅₆H₆₄N₈O₅Zn: 67.63C, 6.49; H, 11.27; N %, Found: C, 67.50; H, 6.55; N, 11.35. MALDI-TOF: m/z 992.52 [M] $^+$. HR-ESI-MS m/z: Calcd for C₅₆H₆₅N₈O₅Zn: 993.4369, Found 993.4282.

Azido-phthalocyanine (11). Monohydroxlated 10 (50 mg, 0.05 mmol) and triethylamine (0.50 mL) were stirred in dichloromethane (2 mL) in an ice bath, then mesyl chloride (0.20 mL) was added drop by drop over 10 min. The stirring continues overnight at room temperature, then the reaction mixture was washed by a dilute solution of potassium carbonate then by water. The organic phase was dried on sodium sulfate. The resulting crude mesylated derivative and NaN₃ (0.5 mmol) are stirred in DMF at 80 °C overnight. CAUTION: NaN₃ must be kept away from acid medium and be handled with care. Water is then added to the cooled reaction mixture and the resulting precipitate is filtrated, recovered in dichloromethane and purified by column chromatography (silica gel) using CH₂Cl₂:EtOH (20:1) as the mobile phase. Yield 90% (46 mg). $C_{56}H_{63}N_{11}O_4Zn$, MW 1019.57. ATR-IR: v_{max} (cm⁻¹) 2924, 2854 (aliph. C-H), 2092 (N₃), 1590 (C=N). ¹H NMR (500 MHz, DMSO- d_6) δ ppm: 0.77–1.05 (m, 9H, CH₃), 1.20–2.37 (m, 34H, CH₂), 4.65, 4.90 (b, 8H, CH₂–O), 7.62–9.08 (m, 12H, ArCH). ¹³C NMR (125 MHz, DMSO- d_6) δ ppm: 14.21, 22.52–32.21, 51.29, 55.44, 68.83, 70.76, 113.30–156.38. Anal. calc. for $C_{56}H_{63}N_{11}O_4Zn$: 65.97C, 6.23; H, 15.11; N %, Found: C, 65.40; H, 6.35; N, 15.45. MALDI-TOF: m/z 1020.50 $[MH]^+$. HR-ESI-MS m/z: Calcd for $C_{56}H_{64}N_{11}O_4Zn$: 1018.4434, Found 1018.4331.

3.4. Synthesis of peptoid-phthalocyanine conjugate

Synthesis of peptoid-phthalocyanine conjugate 1. To a solution of peptoid 5 (13 mg, 0.0180 mmol) and phthalocyanine 11 (20 mg, 0.0216 mmol, 1.2 equiv) dissolved in a biphasic CH2Cl2/H2O (1:1) solvent system (0.5 mL) were added freshly prepared 0.1 M aq. ascorbic acid (0.3 equiv.), and 0.1 M aq. CuSO₄ (0.1 equiv.). After vigorous stirring for 24 h, the mixture was diluted with CH₂Cl₂ (6 mL), washed with water (2 × 1 mL), dried over Na₂SO₄, and concentrated in vacuo. The crude residue was purified first by flash column chromatography (SiO2, 0.1% EtOH in CH₂Cl₂) and then on Bio-Beads S3 stationary phase (CH₂Cl₂), to yield the peptoid-phthalocyanine conjugates 1 (12.4 mg, 40%) as a green powder. TLC: $Rf = 0.63 (9:1 CH_2Cl_2/MeOH)$. ¹H NMR (400 MHz, DMF- d_7) δ (ppm): 0.56–2.32 (m, 91 H, 4 × CH(CH₃)C(CH₃)₃, 3 × $OCH_2(CH_2)_4CH_3$, and $OCH_2(CH_2)_5$), 2.40 (bs, 3 H, $COCH_3$), 3.63–4.86 (m, 20 H, $4 \times OCH_2$, $5 \times NCH_2CO$, and NCH_2 -triazole), 4.88–5.19 (m, 4 H, 4 \times CH(CH₃)C(CH₃)₃), 7.09–9.24 (m, 13 H, 4 \times Ar(CH)₃, and C=CHN-triazole). HRMS (TOF MS ES+) m/z calcd for C₉₅H₁₃₄N₁₇O₁₀⁶⁴Zn $[M+H]^+$ 1736.9785; found 1736.9771. MALDI-TOF: m/z 1735.9712 (calcd. for $C_{95}H_{133}N_{17}O_{10}^{64}Zn$; [M]⁺; found 1735.171).

Synthesis of peptoid-phthalocyanine conjugate 2. To a solution of peptoid 6 (10.5 mg, 0.0084 mmol) and phthalocyanine 11 (25.1 mg, 0.025 mmol, 3 equiv) dissolved in a biphasic CH_2Cl_2/H_2O (1:1) solvent system (0.66 mL) were added freshly prepared 0.1 M aq. ascorbic acid (0.9 equiv.), and 0.1 M aq. $CuSO_4$ (0.3 equiv.). After vigorous stirring for 24 h, the mixture was diluted with CH_2Cl_2 (10 mL), washed with water (2 × 2 mL), dried over Na_2SO_4 , and concentrated in vacuo. The crude residue was purified first by column chromatography (SiO_2 , 0.1% EtOH in CH_2Cl_2) and then by Bio-Beads S3 (THF), to yield the peptoid-phthalocyanine conjugates 2 (17.2 mg, 62%) as a green powder. TLC: $R_f = 0.65$ (9:1 $CH_2Cl_2/MeOH$). ¹H NMR (400 MHz, $DMF-d_7$) δ (ppm):

M. Rzeigui et al. Dyes and Pigments 189 (2021) 109095

0.64–2.62 (m, 173 H, 7 × CH(C H_3)C(C H_3)₃, 6 × OCH₂(C H_2)₄C H_3 , 2 × OCH₂(C H_2)₅ and COCH₃), 3.53–5.33 (m, 45 H, 8 × OCH₂, 9 × NC H_2 CO, 2 × NC H_2 -triazole and 7 × CH(CH₃)C(CH₃)₃), 6.34–9.30 (m, 26 H, 8 × Ar(CH)₃, and 2 × C=CHN-triazole). HRMS (TOF MS ES+) m/z calcd for C₁₈₀H₂₄₈N₃₂O₁₈Zn₂ [M+2H]²⁺ 1636.9023; found 1636.9044. MALDITOF: m/z 3271.790 (calcd. for C₁₈₀H₂₄₆N₃₂O₁₈Zn₂; [M]⁺ 3271.7901).

Synthesis of peptoid-phthalocyanine conjugate 3. The same protocol as for the synthesis of compound **2** was applied to the synthesis of conjugate **3**, which was isolated in 83% yield (22 mg), starting from 10 mg of peptoid **7**. TLC: $R_f = 0.65$ (9:1 CH₂Cl₂/MeOH). ¹H NMR (400 MHz, DMF- d_7) δ (ppm): 0.56–2.65 (m, 173 H, 7 × CH(CH₃)C(CH₃)₃, 6 × OCH₂(CH₂)₄CH₃, 2 × OCH₂(CH₂)₅ and COCH₃), 3.54–5.39 (m, 45 H, 8 × OCH₂, 9 × NCH₂CO, 2 × NCH₂-triazole and 7 × CH(CH₃)C(CH₃)₃), 6.82–9.30 (m, 26 H, 8 × Ar(CH)₃, and 2 × C=CHN-triazole). HRMS (TOF MS ES+) m/z calcd. for C₁₈₀H₂₄₉N₃₂O⁶⁴₁₈Zn₂ [M+3H]³⁺ 1091.6039; found 1091.6047. MALDI-TOF: m/z 3271.790 (calcd. for C₁₈₀H₂₄₆N₃₂O⁶⁴₁₈Zn₂; [M]⁺ 3271.7901).

4. Conclusions

In this work, peptoid oligomers have been used as scaffolds to display phthalocyanines dyes. In this way, the first synthesis and analysis of the photoproperties of peptoid-phthalocyanine conjugates has been achieved. The peptoid oligomers with aliphatic side chains to prevent aromatic interactions were designed to adopt the PolyProline type I conformation characterized by cis-amide bonds and the phthalocyanines were grafted by CuAAC reactions. Very importantly, the helix content of the peptoids is conserved upon phthalocyanine grafting, allowing for an accurate comparison of the photoproperties of the conjugates. Measurements of the electronic absorption and fluorescence spectra of the conjugates and of a monomeric reference phthalocyanine showed that the presence of the peptoid backbone has no effect on the photoproperties of the phthalocyanines. Conjugates in which two phthalocyanine units are grafted on a same peptoid backbone exhibit intramolecular aggregation behaviour, due to the fact that the two phthalocyanines are kept close to each other, quite independently of their relative position on the peptoid backbone, probably due to the important flexibility of the spacer used. Further works with more rigid spacers between the phthalocyanine and the helix backbone should allow to better control the interactions between the macrocycles.

Author statement

Maha Rzeigui, Zeynel Şahin, Olivier Roy, Tuğba Küçük, Ömer Göler, Devrim Atilla made the syntheses and characterizations.

Fabienne Dumoulin, Claude Tailllefumier and Jameleddine Khiari conceived and supervised the work.

Declaration of competing interest

The authors declare that they have no known competing financial interests or personal relationships that could have appeared to influence the work reported in this paper.

Acknowledgments

We thank Aurélie Job for HPLC measurements and Martin Leremboure (UCA Partner) for LCMS. M.R. was supported by a grant from the Ministry for Higher Education and Scientific Research of Tunisia. We acknowledge use of the UMS2008-IBSLor Biophysics and Structural Biology core facility at Université de Lorraine for CD measurements.

Appendix A. Supplementary data

Supplementary data to this article can be found online at https://doi. org/10.1016/j.dyepig.2020.109095.

References

- [1] Rio Y, Rodríguez-Morgade MS, Torres T. Modulating the electronic properties of porphyrinoids: a voyage from the violet to the infrared regions of the electromagnetic spectrum. Org Biomol Chem 2008;6:1877–94.
- [2] Senge MO, Ryan AA, Letchford KA, MacGowan SA, Mielke T. Chlorophylls, symmetry, chirality, and photosynthesis. Symmetry 2014;6:781–843.
- [3] a) Poulos TL. Heme enzyme structure and function. Chem Rev 2014;114:3919–62.
 b) Erdogan H. One small step for cytochrome P450 in its catalytic cycle, one giant leap for enzymology. J Porphyr Phthalocyanines 2019;23:358–66.
- [4] Craig GW. Total synthesis of vitamin B12 a fellowship of the ring. J Porphyr Phthalocyanines 2015;20:1–20.
- [5] Zhang B, Sun L. Artificial photosynthesis: opportunities and challenges of molecular catalysts. Chem Soc Rev 2019;48:2216–64.
- [6] a) Sorokin AB. Phthalocyanine metal complexes in catalysis. Chem Rev 2013;113: 8152–91.b) Costentin C, Robert M, Savéant JM. Current issues in molecular catalysis illustrated by iron porphyrins as catalysts of the CO₂-to-CO electrochemical conversion. Acc Chem Res 2015;48:2996–3006.c) Kariyawasam K, Ricoux R, Mahy J-P. Recent advances in the field of artificial hemoproteins: new efficient eco-compatible biocatalysts for nitrene-, oxene- and carbene-transfer reactions. J Porphyr Phthalocyanines 2019;23:1273–85.
- [7] Fukuzumi S, Lee Y-M, Nam W. Photocatalytic redox reactions with metalloporphyrins. J Porphyr Phthalocyanines 2020;2:21–32.
- [8] a) Lo PC, Rodriguez-Morgade MS, Pandey RK, Ng DKP, Torres T, Dumoulin F. The unique features and promises of phthalocyanines as advanced photosensitisers for photodynamic therapy of cancer. Chem Soc Rev 2020;49:1041–56.b) Frochot C, Mordon S. Update of the situation of clinical photodynamic therapy in Europe in the 2003–2018 period. J Porphyr Phthalocyanines 2019;23:347–57.c) Li X, Zheng B-D, Peng X-H, Li S-Z, Ying J-W, Zhao Y, Huang J-D, Yoon J. Phthalocyanines as medicinal photosensitizers: developments in the last five years. Coord Chem Rev 2019:379:147–60.
- [9] Urbani M, Ragoussi ME, Nazeeruddin MK, Torres T. Phthalocyanines for dyesensitized solar cells. Coord Chem Rev 2019;381:1–64.
- [10] El-Khouly ME, Ito O, Smith PM, D'Souza F. Intermolecular and supramolecular photoinduced electron transfer processes of fullerene-porphyrin/phthalocyanine systems. J Photochem Photobiol C Photochem Rev 2004;5:79–104.
- [11] González-Rodríguez D, Giovanni Bottari G. Phthalocyanines, subphthalocyanines and porphyrins for energy and electron transfer applications. J Porphyr Phthalocyanines 2009;13:624–36.
- [12] Llansola-Portoles MJ, Gust D, Moore TA, Moore AL. Artificial photosynthetic antennas and reaction centers. Compt Rendus Chem 2017;20:296–313.
- [13] Ryan A, Gehrold A, Perusitti R, Pintea M, Fazekas M, Locos OB, Blaikie F, Senge MO. Porphyrin dimers and arrays. Eur J Org Chem 2011;2011:5817–44.
- [14] Tanaka T, Osuka A. Conjugated porphyrin arrays. synthesis, properties and applications for functional materials. Chem Soc Rev 2015;44:943–69.
- [15] Medforth CJ, Wang Z, Martin KE, Song Y, Jacobsen JL, Shelnutt JA. Self-assembled porphyrin nanostructures. Chem Commun 2009:7261–77.
- [16] Drain CM, Varotto A, Radivojevic I. Self-organized porphyrinic materials. Chem Rev 2009;109:1630–58.
- [17] Imahori H, Umeyama T, Kurotobi K, Takano Y. Self-assembling porphyrins and phthalocyanines for photoinduced charge separation and charge transport. Chem Commun 2012;48:4032–45.
- [18] a) Fathalla M, Neuberger A, Li SC, Schmehl R, Diebold U, Jayawickramarajah J. Straightforward self-assembly of porphyrin nanowires in water: harnessing adamantane/β-cyclodextrin interactions. J Am Chem Soc 2010;132:9966–7.b) Prigorchenko E, Ustrnul L, Borovkov V, Aav R. Heterocomponent ternary supramolecular complexes of porphyrins: a review. J Porphyr Phthalocyanines 2019;23:1308–25.
- [19] Kang B, Chung S, Ahn YD, Lee J, Seo J. Porphyrin-peptoid conjugates: face-to-face display of porphyrins on peptoid helices. Org Lett 2013;15:1670–3.
- [20] Zuckermann RN. Peptoid origins. Biopolymers 2011;96:545–55.
- [21] (a) Kwon YU, Kodadek T. Quantitative evaluation of the relative cell permeability of peptoids and peptides. J Am Chem Soc 2007;129:1508–9 (b) Vollrath SBL, Furniss D, Schepers U, Brase S. Amphiphilic peptoid transporters - synthesis and evaluation. Org Biomol Chem 2013;11:8197–201.
- [22] Miller SM, Simon RJ, Ng S, Zuckermann RN, Kerr JM, Moos WH. Comparison of the proteolytic susceptibilities of homologous L-amino-acid, D-amino-acid, and Nsubstituted Glycine peptide and peptoid oligomers. Drug Dev Res 1995;35:20–32.
- [23] Zuckermann RN, Kerr JM, Kent SBH, Moos WH. Efficient method for the preparation of peptoids [oligo(N-substituted glycines)] by submonomer solid-phase synthesis. J Am Chem Soc 1992;114:10646–7.
- [24] Culf AS, Ouellette RJ. Solid-phase synthesis of N-substituted Glycine oligomers (alpha-Peptoids) and derivatives. Molecules 2010;15:5282–335.
- [25] (a) Patch JA, Kirshenbaum K, Seurynck SL, Zuckermann RN, Barron AE. Versatile oligo(N-substituted) glycines: the Many roles of peptoids in drug discovery. In: Nielson PE, editor. Pseudo-peptides in drug development. Germany: Wiley-VCH Weinheim; 2004.(b) Zuckermann RN, Kodadek T. Peptoids as potential therapeutics. Curr Opin Mol Therapeut 2009;11:299–307.
- [26] (a) Knight AS, Zhou EY, Francis MB, Zuckermann RN. Sequence programmable peptoid polymers for diverse materials applications. Adv Mater 2015;27:5665–91. (b) Gangloff N, Ulbricht J, Lorson T, Schlaad H, Luxenhofer R. Peptoids and polypeptoids at the frontier of supra- and macromolecular engineering. Chem Rev 2016;116:1753–802.
- [27] Sui Q, Borchardt D, Rabenstein DL. Kinetics and equilibria of cis/trans isomerization of backbone amide bonds in peptoids. J Am Chem Soc 2007;129: 12042–8.

- [28] (a) Gorske BC, Bastian BL, Geske GD, Blackwell HE. Local and tunable n ->pi* interactions regulate amide isomerism in the peptoid backbone. J Am Chem Soc 2007;129:8928-9.(b) Gorske BC, Stringer JR, Bastian BL, Fowler SA, Blackwell HE. New strategies for the design of folded peptoids revealed by a survey of noncovalent interactions in model systems. J Am Chem Soc 2009;131:16555-67. (c) Caumes C, Roy O, Faure S, Taillefumier C. The click triazolium peptoid side chain. A strong cis-amide inducer enabling chemical diversity. J Am Chem Soc 2012;134:9553-6.(d) Roy O, Caumes C, Esvan Y, Didierjean C, Faure S, Taillefumier C. The tert-butyl side chain: a powerful means to lock peptoid amide bonds in the cis conformation. Org Lett 2013;15:2246-9.(e) Angelici G, Bhattacharjee N, Roy O, Faure S, Didierjean C, Jouffret L, Jolibois F, Perrin L, Taillefumier C. Weak backbone CH···O=C and side chain tBu···tBu London interactions help promote helix folding of achiral NtBu peptoids. Chem Commun 2016;52:4573-6. Gimenez D, Aguilar JA, Bromley EH, Cobb SL.(f) Stabilising peptoid helices using non-chiral fluoroalkyl monomers. Angew Chem Int Ed 2018; 57:10549–53.(g) Wijaya AW, Nguyen AI, Roe LT, Butterfoss GL, Spencer RK, Li NK, Zuckermann RN. Cooperative intramolecular hydrogen bonding strongly enforces cis-peptoid folding. J Am Chem Soc 2019;141:19436-47.
- [29] (a) Horne WS. Peptide and peptoid foldamers in medicinal chemistry. Expet Opin Drug Discov 2011;6:1247–62.(b) Mandity IM, Fulop F. An overview of peptide and peptoid foldamers in medicinal chemistry. Expet Opin Drug Discov 2015;10: 1163–77.
- [30] (a) Huang K, Wu CW, Sanborn TJ, Patch JA, Kirshenbaum K, Zuckermann RN, Barron AE, Radhakrishnan I. A threaded loop conformation adopted by a family of peptoid nonamers. J Am Chem Soc 2006;128:1733–8.(b) Crapster JA, Guzei IA, Blackwell HE. A peptoid ribbon secondary structure. Angew Chem Int Ed 2013;52: 5079–84.(c) Gorske BC, Mumford EM, Conry RR. Tandem incorporation of enantiomeric residues engenders discrete peptoid structures. Org Lett 2016;18: 2780–3.(d) Gorske BC, Mumford EM, Gerrity CG, Ko I. A peptoid square helix via synergistic control of backbone dihedral angles. J Am Chem Soc 2017;139:8070–3. (e) Dumonteil G, Bhattacharjee N, Angelici G, Roy O, Faure S, Jouffret L, Jolibois F, Perrin L, Taillefumier C. Exploring the conformation of mixed cis-trans α,β-oligopeptoids: a joint experimental and computational study. J Org Chem 2018;83:6382–96.
- [31] Shah NH, Butterfoss GL, Nguyen K, Yoo B, Bonneau R, Rabenstein DL, Kirshenbaum K. Oligo(N-aryl glycines). A new twist on structured peptoids. J Am Chem Soc 2008;130:16622–32. Stringer JR, Crapster JA, Guzei IA, Blackwell HE. Construction of Peptoids with All Trans-Amide Backbones and Peptoid Reverse Turns via the Tactical Incorporation of N-Aryl Side Chains Capable of Hydrogen Bonding. J Org Chem 2010;75:6068-6078. Mannige RV, Haxton TK, Proulx C, Robertson EJ, Battigelli A, Butterfoss GL, Zuckermann RN, Whitelam S. Peptoid nanosheets exhibit a new secondary-structure motif. Nature 2015;526:415-420.
- [32] (a) Stringer JR, Crapster JA, Guzei IA, Blackwell HE. Extraordinarily robust polyproline type I peptoid helices generated via the incorporation of alpha-chiral aromatic N-1-Naphthylethyl side chains. J Am Chem Soc 2011;133:15559–67.(b) Roy O, Dumonteil G, Faure S, Jouffret L, Kriznik A, Taillefumier C. Homogeneous and robust polyproline type I helices from peptoids with nonaromatic alpha-chiral side chains. J Am Chem Soc 2017;139:13533–40.(c) Zborovsky L, Smolyakova A, Baskin M, Maayan G. A pure polyproline type I-like peptoid helix by metal coordination. Chem Eur J 2018;24:1159–67.
- [33] (a) Wu CW, Sanborn TJ, Huang K, Zuckermann RN, Barron AE. Peptoid oligomers with α-chiral, aromatic side chains. Sequence requirements for the formation of stable peptoid helices. J Am Chem Soc 2001;123:6778–84.(b) Wu CW, Sanborn TJ, Zuckermann RN, Barron AE. Peptoid oligomers with α-chiral, aromatic

- side chains. Effects of chain length on secondary structure. J Am Chem Soc 2001; 123:2958-63.
- [34] (a) Wu CW, Kirshenbaum K, Sanborn TJ, Patch JA, Huang K, Dill KA, Zuckermann RN, Barron AE. Structural and spectroscopic studies of peptoid oligomers with α-chiral aliphatic side chains. J Am Chem Soc 2003;125:13525–30. (b) Rzeigui M, Traikia M, Jouffret L, Kriznik A, Khiari J, Roy O, Taillefumier C. Strengthening peptoid helicity through sequence site-specific positioning of amide cis-inducing NtBu monomers. J Org Chem 2020;85:2190–201.
- [35] Shyam R, Nauton L, Angelici G, Roy O, Taillefumier C, Faure S. NCα-gemdimethylated peptoid side chains: a novel approach for structural control and peptide sequence mimetics. Biopolymers 2019:e23273.
- [36] Luo Y, Song Y, Wang M, Jian T, Ding S, Mu P, Liao Z, Shi Q, Cai X, Jin H, Du D, Dong WJ, Chen CL, Lin Y. Bioinspired peptoid nanotubes for targeted tumor cell imaging and chemo-photodynamic therapy. Small 2019;15:1902485.
- [37] Schröder T, Schmitz K, Niemeier N, Balaban TS, Krug HF, Schepers U, Bräse S. Solid-phase synthesis, bioconjugation, and toxicology of novel cationic oligopeptoids for cellular drug delivery. Bioconjugate Chem 2007;18:342–54.
- [38] Kim Y, Kang B, Ahn HY, Seo J, Nam KT. Plasmon enhanced fluorescence based on porphyrin-peptoid hybridized gold nanoparticle platform. Small 2017;13:1700071.
- [39] Yang W, Kang B, Voelz VA, Seo J. Control of porphyrin interactions via structural changes of a peptoid scaffold. Org Biomol Chem 2017;15:9670–9.
- [40] Lee YJ, Kang B, Seo J. Metalloporphyrin dimers bridged by a peptoid helix: hostguest interaction and chiral recognition. Molecules 2018;23:2741.
- [41] Yang W, Jo J, Oh H, Lee H, Chung Wj, Seo J. Peptoid helix displaying flavone and porphyrin: synthesis and intramolecular energy transfer. J Org Chem 2020;85: 1392–400
- [42] Kang B, Yang W, Lee S, Mukherjee S, Forstater J, Kim H, Goh B, Kim TY, Voelz VA, Pang Y, Seo J. Precisely tuneable energy transfer system using peptoid helix-based molecular scaffold. Sci Rep 2017;7:4786.
- [43] Topal SZ, Ü Işci, Kumru U, Atilla D, Gürek AG, Hirel C, Durmuş M, Tommasino JB, Luneau D, Berber S, Dumoulin F, Ahsen V. Modulation of the electronic and spectroscopic properties of Zn(II) phthalocyanines by their substitution pattern. Dalton Trans 2014;43:6897–908.
- [44] Kobayashi N, Narita F, Ishii K, Muranaka A. Optically active oxo (phthalocyaninato)vanadium(IV) with geometric asymmetry: synthesis and correlation between the circular dichroism sign and conformation. Chem Eur J 2009;15:10173–81.
- [45] Kolb HC, Finn MG, Sharpless KB. Click chemistry: diverse chemical function from a few good reactions. Angew Chem Int Ed 2001;40:2004–21.
- [46] Acherar S, Colombeau L, Frochot C, Vanderesse R. Synthesis of porphyrin, chlorin and phthalocyanine derivatives by azide-alkyne click chemistry. Curr Med Chem 2015;22:3217–54.
- [47] Dumoulin F, Ahsen V. Click chemistry: the emerging role of the azide-alkyne Huisgen dipolar addition in the preparation of substituted tetrapyrrolic derivatives. J Porphyr Phthalocyanines 2011;15:481–504.
- [48] Aliouat H, Caumes C, Roy O, Zouikri M, Taillefumier C, Faure S. 1,2,3-Triazolium-Based peptoid oligomers. J Org Chem 2017;82:2386–98.
- [49] Lee BY, Park SR, Jeon HB, Kim KS. A new solvent system for efficient synthesis of 1,2,3-triazoles. Tetrahedron Lett 2006;47:5105–9.
- [50] George RD, Snow AW. Synthesis of 3-nitrophthalonitrile and tetra-α-substituted phthalocyanines. J Heterocycl Chem 1995;32:495–8.
- [51] Wang Z, Gai S, Wang C, Yang G, Zhong C, Dai Y, He F, Yan D, Yang P. Self-assembled zinc phthalocyanine nanoparticles as excellent photothermal/photodynamic synergistic agent for antitumor treatment. Chem Eng J 2019;361: 117–28